The effect of Ca and Th substitution on the crystal-field spectrum of the high-T_c superconductor $HoBa_2Cu_3O_x$

2002 J. Phys.: Condens. Matter 14 1923

(http://iopscience.iop.org/0953-8984/14/8/320)

INSTITUTE OF PHYSICS PUBLISHING JOURNAL OF PHYSICS: CONDENSED MATTER

J. Phys.: Condens. Matter **14** (2002) 1923–1936 PII: S0953-8984(02)28203-X

The effect of Ca and Th substitution on the crystal-field spectrum of the high-T_c superconductor $HoBa_2Cu_3O_x$

N Golosova[1], A Podlesnyak[1,2,3], E Mitberg[1], V Bobrovskii[1], A Mirmelstein[1] and A Furrer[2]

[1] Institute for Metal Physics, Russian Academy of Sciences, Ural Branch, 18 S Kovalevskaya Street, 620219 Ekaterinburg GSP-170, Russia
[2] Laboratory for Neutron Scattering, ETH Zürich and Paul Scherrer Institute, CH-5232 Villigen PSI, Switzerland

E-mail: andrew.podlesnyak@psi.ch

Received 22 August 2001, in final form 21 January 2002
Published 15 February 2002
Online at stacks.iop.org/JPhysCM/14/1923

Abstract

The inelastic neutron scattering technique was employed to study the transitions between the low-lying levels of the ground-state J-multiplet of the Ho^{3+} ions in $Ho_{1-y}Ca_yBa_2Cu_3O_x$ ($x \approx 6.3, 7.0$; $y \approx 0.1, 0.2$) and $Ho_{1-y}Th_yBa_2Cu_3O_x$ ($x \approx 6.3$; $y \approx 0.07, 0.13$) split by the crystalline electric field. For oxygen-rich Ca-doped samples, the observed energy spectra exhibit a fine structure, which reflects the behaviour of the local hole density near the doping centre. For the first time this experimental observation unambiguously confirms that the charge inhomogeneity, which was found to be a characteristic feature of the underdoped cuprates, still exists in the deeply overdoped regime with $T_c = 56$ K. On the other hand, the modification of the crystal-field spectra observed for the oxygen-deficient samples with both Ca^{2+} and Th^{4+} substitutions for Ho^{3+} is found to result from distortions of the copper–oxygen polyhedron around the Ho^{3+} ion in the direct neighbourhood of the implanted ions, rather than from the doping-induced variation of the carrier concentration in the CuO_2 planes.

1. Introduction

Experimental studies of fine effects in the CuO_2 planes resulting from doping of copper oxide superconductors with charge carriers can enhance our understanding of both the normal and the superconducting states in high-T_c compounds. The inhomogeneous distribution of the doping-induced charge carriers is of particular interest. It was shown theoretically that the

[3] Author to whom any correspondence should be addressed.

presence of holes makes layered antiferromagnets unstable against phase separation into hole-rich and hole-poor regions at intermediate length scales [1–6]. At the same time, there is growing experimental evidence for mesoscopic striped phases and their effect on the electronic properties in perovskite materials [7–16]. It is therefore of crucial interest to obtain direct experimental information on the charge distribution within the superconducting CuO_2 planes of high-T_c cuprates. Since in most rare-earth-based (R-based) high-T_c compounds the R ions are situated close to the CuO_2 planes, the crystalline-electric-field (CEF) interaction at the R site constitutes an ideal probe of the local symmetry as well as the local charge distribution, and thereby directly monitors the variation of the carrier concentration induced by doping [17]. The inelastic neutron scattering (INS) technique is a valuable tool for investigating the CEF excitations in optically opaque high-T_c compounds. This technique allows one to obtain unique experimental information on the peculiarities of the charge-transfer process and the cluster formation upon doping (which may be called 'frustrated phase separation') [18–23] as well as on the symmetry of the gap function of high-T_c superconductors [24, 25].

The phenomenon of frustrated phase separation reflects a remarkable difference between the average carrier concentration and the local hole density in the CuO_2 planes near the doping centres. Already, by means of neutron spectroscopy of the CEF interaction, cluster formation upon doping of the $RBa_2Cu_3O_x$ (R = rare earth) high-T_c superconductors was firmly established for the case of R = Er, the doping being induced by the variation of the oxygen concentration ($6 < x < 7$) [17, 22]. Only limited experimental information was obtained for Ca-doped $ErBa_2Cu_3O_{\approx 7}$ (positive doping) [26, 27]. To our knowledge there is no experimental information about negative doping, which can be achieved by substitution of Th^{4+} ions for R^{3+} ions. Therefore, it is of general interest to investigate whether this effect depends on the way in which one induces the doping or not.

The aim of the present work is thus the INS investigation of the effect of the in-plane doping on the CEF spectrum of $HoBa_2Cu_3O_x$ in the underdoped (low-oxygen-concentration, $x \approx 6.3$) and overdoped (high-oxygen-concentration, $x \approx 7$) regimes. The in-plane doping is induced either by substitution of Ca^{2+} ions (positive doping [28]) or Th^{4+} ions (negative doping [29]) for Ho^{3+} ions. The CEF spectra for both $HoBa_2Cu_3O_x$ [23] and $ErBa_2Cu_3O_x$ [21, 22] are fully established for the whole range of oxygen concentration $6 < x < 7$. We have chosen $HoBa_2Cu_3O_x$ for our study because the CEF spectrum of the Ho^{3+} ions consists of singlets only in the orthorhombic phase; thus a more unambiguous interpretation of the experimental spectra may be expected compared to the case for $ErBa_2Cu_3O_x$. The results obtained give direct evidence for charge inhomogeneity in overdoped $HoBa_2Cu_3O_7$ ($T_c = 56$ K), whereas for underdoped $HoBa_2Cu_3O_{6.3}$ the observed CEF spectra can be understood in terms of structural distortions alone.

2. Sample preparation and characterization

The ceramic samples of $Ho_{1-y}M_yBa_2Cu_3O_x$ (M = Ca, Th) were synthesized by solid-state reaction starting with high-purity Ho_2O_3, ThO_2, CuO oxides and $CaCO_3$, and $BaCO_3$ carbonates. The appropriate mixtures of reagents were ground with the addition of ethanol and heated in vacuum at 820–850 °C for 20 h until complete decomposition of carbon dioxides was achieved. Further calcination was carried out in air at 900–960 °C for 80 h with intermediate grindings and pressings into pellets. The samples were finally reacted for a few hours at 1000 °C in flowing oxygen at 1 bar and then slowly cooled down to 350 °C. The last high-temperature reaction was used to minimize the $BaCuO_2$ and $Ba_4CaCu_3O_8$ impurities [30]. By these means, Ca is forced to substitute primarily at the R sites, and heavily overdoped samples (x close to 7) can be obtained. The prepared samples were then separated into two groups.

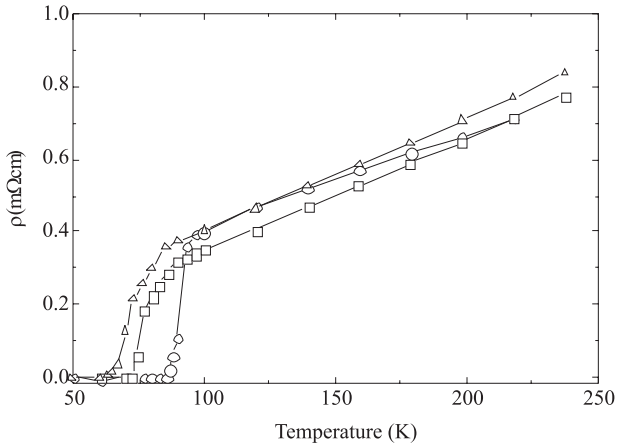

Figure 1. The temperature dependence of the electrical resistivity ρ of the $Ho_{1-y}Ca_yBa_2Cu_3O_{\approx 7}$ samples measured by a standard four-probe technique. Circles, squares, and triangles represent the data for $y = 0$, 0.1, and 0.25, respectively.

The first group, with the compositions $Ho_{1-y}Ca_yBa_2Cu_3O_{\approx 7}$ ($y = 0$, 0.1, and 0.25), were considered to lie in the optimally doped and overdoped regimes. The second group, with the compositions $Ho_{1-y}Ca_yBa_2Cu_3O_x$ ($y = 0$, 0.1, and 0.22) and $Ho_{1-y}Th_yBa_2Cu_3O_x$ ($y = 0$, 0.07, and 0.13), were annealed in evacuated atmosphere ($p_{O_2} = 10^2$ Pa) at 640 °C and then quenched into liquid gallium. Since the expected value of x for these samples is about 6.3, they are in the underdoped regime. Although the Ca concentrations $y = 0.22$ and 0.25 most probably exceed the solubility limit $y \approx 0.2$ [30], we deliberately synthesized these samples to enhance the expected effects, taking it into account that the CEF spectrum of the 123-phase cannot be affected by a small amount ($\sim$ a few per cent) of impurity phase.

The samples were characterized first by x-ray powder diffraction. The specimens with Ca contents $y = 0$, 0.1 turn out to be of single phase within the limit of the experimental uncertainty. Only the samples with a higher Ca concentrations ($y = 0.22$, 0.25) showed a small amount of $BaCuO_2$ (less than 1%). AC susceptibility measurements were used to detect the superconducting transition temperatures: $T_c \sim 92$, 71, and 56 K for $Ho_{1-y}Ca_yBa_2Cu_3O_{\approx 7}$ ($y = 0$, 0.1, 0.25), respectively, in agreement with the data obtained by other groups [26, 30]. The low-oxygen compositions were found to be non-superconducting above 4.2 K for both Ca and Th substitutions. Therefore, they are far into the low-doping regime.

To ensure that the fully oxidized samples $Ho_{1-y}Ca_yBa_2Cu_3O_{\approx 7}$ ($y = 0.1$, 0.25) were in the overdoped regime, their electrical resistivities was measured by the standard four-probe technique (figure 1). Both the absolute values of the resistivities as well as their temperature dependences for Ca-doped samples provide evidence of overdoped behaviour (e.g., compare figure 1 of the present paper with figure 3 of [31]). Measurements of the static magnetic susceptibility, often used to confirm that samples are in the overdoped regime, can hardly be used in our case, since a large contribution to the susceptibility due to Ho^{3+} ions masks the absence of the pseudogap behaviour, which is considered to be a prominent sign of a sample being in the overdoped region.

Further characterization of the $Ho_{1-y}Ca_yBa_2Cu_3O_x$ samples follows from the structural study. The DMC neutron powder diffractometer at SINQ (PSI, Switzerland) was used for the structural determination. The neutron powder diffraction patterns were recorded at $T = 9$ K in a 2Θ angular range between 8° and 87.8° with a 2Θ step of 0.2° and a wavelength

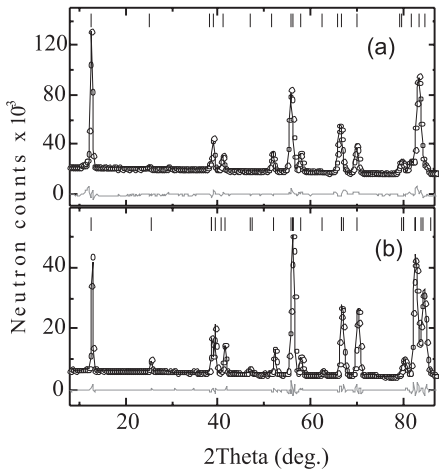

Figure 2. Observed, calculated, and difference neutron diffraction patterns of $Ho_{0.9}Ca_{0.1}Ba_2Cu_3O_x$ with low ($x = 6.24$, panel (*a*)) and high ($x = 6.99$, panel (*b*)) oxygen concentration.

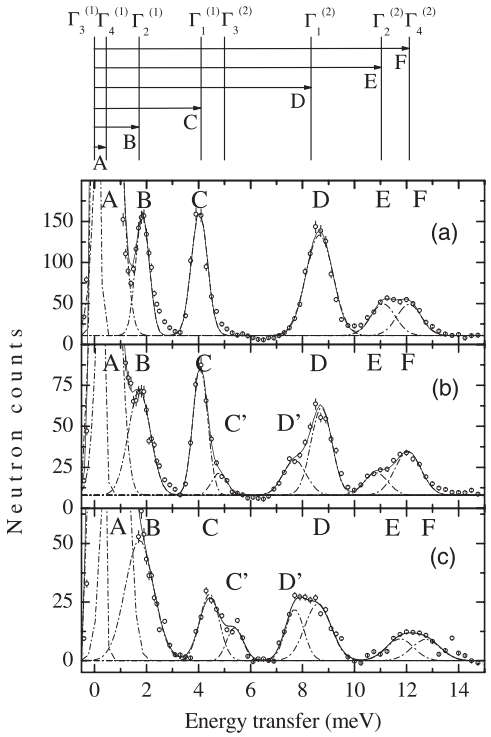

Figure 3. Energy spectra of neutrons scattered from $Ho_{1-y}Ca_yBa_2Cu_3O_{\approx 7}$ ($T = 1.5$ K, $Q = 1.8$ Å^{-1}, $E_f = 7$ meV) for $y = 0$, 0.1, 0.25 (in panels (*a*), (*b*), (*c*), respectively). The curves are the result of a least-squares fitting procedure (table 2) with use of Gaussian functions to describe the lineshape of the CEF transitions. The CEF transitions are denoted as explained in the text. The top of the figure shows the CEF splitting of $HoBa_2Cu_3O_7$ [20], and the observed transitions are indicated by arrows.

Table 1. Refined structural parameters for $Ho_{1-y}Ca_yBa_2Cu_3O_x$ with low and high oxygen concentration. The hole concentration V_- (hole/plane) is calculated according to [35] via the bond valence sums [36] as described in the text. $s = 2(b-a)/(a+b)$ denotes the orthorhombic strain. $N(\mathrm{Ca}) = y$, $N(\mathrm{O(4)} + \mathrm{O(5)}) + 6 = x$.

x		6.29	6.24	6.32	6.95	6.99	6.86
y		0	0.1	0.22	0	0.1	0.25
a (Å)		3.8555(2)	3.8558(3)	3.8558(3)	3.8179(2)	3.8180(3)	3.8183(4)
b (Å)		3.8555(2)	3.8558(3)	3.8558(3)	3.8828(2)	3.8751(3)	3.8699(5)
c (Å)		11.7691(5)	11.7602(5)	11.7622(5)	11.6343(5)	11.6445(6)	11.6667(8)
s		0	0	0	0.0169	0.0148	0.0134
Ho	B	0.09(1)	0.12(1)	0.12(1)	0.11(1)	0.15(4)	0.75(4)
	N		0.90(2)	0.78(1)		0.904(6)	0.754(8)
Ca	B		0.12(1)	0.12(1)		0.15(4)	0.75(4)
	N		0.10(2)	0.22(2)		0.096(6)	0.246(8)
Ba	z	0.1946(2)	0.1949(3)	0.1952(3)	0.1832(3)	0.1833(8)	0.1865(8)
	B	0.122(2)	0.122(2)	0.128(4)	0.141(3)	0.16(4)	0.77(4)
Cu(1)	B	0.15(1)	0.15(1)	0.15(1)	0.51(2)	0.9(3)	0.9(3)
Cu(2)	z	0.3618(2)	0.3617(3)	0.3615(4)	0.3552(2)	0.3563(7)	0.3574(1)
	B	0.15(1)	0.15(1)	0.15(1)	0.51(2)	0.9(3)	0.9(3)
O(1)	z	0.1535(2)	0.1529(3)	0.1504(2)	0.1598(3)	0.1600(9)	0.1585(9)
	B	0.7(4)	1.4(7)	0.7(4)	0.4(2)	1.5(2)	1.3(2)
O(2)	z	0.3773(2)	0.3785(4)	0.3805(1)	0.3776(3)	0.3789(5)	0.3796(5)
	B	0.7(4)	1.4(7)	0.7(4)	0.4(2)	1.5(2)	1.3(2)
O(3)	z				0.3768(3)	0.3752(5)	0.3732(5)
	B				0.4(1)	1.5(2)	1.3(2)
O(4)	B	0.7	1.8(7)	0.7(4)	0.5(2)	0.5(2)	0.8(2)
	N	0.29(2)	0.24(2)	0.32(1)	0.89(1)	0.94(1)	0.76(2)
O(5)	B				0.5(2)	0.5(2)	0.8(2)
	N				0.06(3)	0.05(3)	0.10(3)
R_B	(%)	3.18	5.45	3.39	1.68	1.79	2.88
R_f	(%)	3.61	4.99	3.92	1.06	1.11	1.88
R_{exp}	(%)	1.87	1.71	2.13	1.82	1.91	2.03
V_-		−0.024(3)	−0.024(6)	−0.012(6)	0.188(4)	0.234(5)	0.258(6)

$\lambda = 2.5603$ Å. The structures were refined using the profile refinement program FullProf [32]. As an example, figure 2 shows the observed, calculated, and difference neutron diffraction patterns for $Ho_{0.9}Ca_{0.1}Ba_2Cu_3O_x$ ($x \approx 6.24, 6.99$). All of the samples under study with low oxygen concentration are found to belong to the tetragonal $P4/mmm$ space group, while the optimally doped and overdoped Ho-123 samples are described in the orthorhombic $Pmmm$ space group. The structural parameters for the $Ho_{1-y}Ca_yBa_2Cu_3O_x$ derived from the profile refinement are given in table 1. At low oxygen concentration, Ca substitution causes rather subtle structural variations. At high oxygen concentration, Ca substitution leads to a decrease of the orthorhombic strain $s = 2(b-a)/(a+b)$, where a and b are the in-plane lattice parameters (see table 1). The lattice parameter c increases with y in the overdoped regime. Such a behaviour of the structural parameters for the Ca-substituted overdoped 123 compounds agrees with earlier results [26]. Note that the refinement of the Ca concentration is possible due to the large difference in neutron scattering length between Ca and Ho nuclei. Detailed results of the structural investigation of the $Ho_{1-y}Th_yBa_2Cu_3O_x$ will be described elsewhere [33].

Table 2. Energies E_i and relative transition intensities I_i/I_A of the CEF spectra for $HoBa_2Cu_3O_x$ at different doping levels derived from the present INS experiments by a least-squares fitting procedure as described in the text. The excited CEF levels are denoted by A–F as indicated in figures 3 and 5.

	A	B	C	D	E	F
Undoped $HoBa_2Cu_3O_{6.3}$						
E_{obs} (meV)	1.1(1)		—	7.50(5)	10.9(1)	
E_{calc} (meV)	1.10		4.89	7.47	10.85	
$I_i/I_{A\,obs}$	1		—	0.43(4)	0.30(4)	
$I_i/I_{A\,calc}$	1		0	0.62	0.36	
Optimally doped $HoBa_2Cu_3O_{6.95}$						
E_{obs} (meV)	0.42(2)	1.8(1)	4.04(2)	8.61(2)	11.1(3)	12.1(3)
E_{calc} (meV)	0.45	1.72	4.10	8.33	11.02	12.11
$I_i/I_{A\,obs}$	1	0.23(3)	0.25(5)	0.35(5)	0.2(1)	0.2(1)
$I_i/I_{A\,calc}$	1	0.22	0.30	0.47	0.15	0.21
$Ho_{0.75}Ca_{0.25}Ba_2Cu_3O_{6.95}$, extrapolated from $HoBa_2Cu_3O_{6.95}$ according to equation (6)						
E_{calc} (meV)	0.51	1.77	4.45	8.25	11.07	12.14
$I_i/I_{A\,calc}$	1	0.24	0.32	0.47	0.18	0.22
	A′	B′	C′	D′	E	F
Overdoped component of $Ho_{0.75}Ca_{0.25}Ba_2Cu_3O_{6.86}$						
E_{obs} (meV)	0.76(3)	1.15(5)	5.4(2)	7.7(2)	11.9(3)	12.8(3)
E_{calc} (meV)	0.63	1.13	5.60	7.39	11.9	12.2
$I_i/I_{A'\,obs}$	1	0.64(6)	—	—		
$I_i/I_{A'\,calc}$	1	0.59	—	—		

3. Crystal-field spectra

3.1. Experimental procedure

The triple-axis spectrometer DrüchaL at SINQ (PSI, Switzerland) was used to determine the CEF transitions of the ground-state J-multiplet $^5I_8$ of the Ho^{3+} ions in the samples under study. The CEF of tetragonal symmetry ($x = 6.3$) splits the Ho^{3+} ground-state multiplet into nine singlets and four doublets. Eight levels, including two doublets, were found in a low-energy window ($\Delta E < 12$ meV) and nine levels, including two doublets, in a high-energy window ($55 < \Delta E < 74$ meV) [23]. The transition into the orthorhombic phase causes an additional splitting of the doublets, with the result that all the CEF levels become singlets [23]. Since the energies of the low-lying levels are most sensitive to the doping, in the present study we focus on the low-energy part of the experimental spectra. High-resolution energy scans up to an energy transfer $\Delta E = 3.0$ meV were recorded at temperature $T = 1.5$ K, modulus of the scattering vector $Q = 0.85$ Å^{-1}, and scattered energy $E_f = 3.5$ meV. A Be filter was used to reduce high-order contamination. Some additional spectra were measured up to an energy transfer $\Delta E = 15$ meV at 1.5 K with $Q = 1.8$ Å^{-1} and $E_f = 7$ meV.

3.2. Overdoped regime

Energy spectra of neutrons scattered from $HoBa_2Cu_3O_{6.95}$, $Ho_{0.9}Ca_{0.1}Ba_2Cu_3O_{6.99}$, and $Ho_{0.75}Ca_{0.25}Ba_2Cu_3O_{6.86}$ at $T = 1.5$ K are shown in figures 3 and 4. As expected, the low-energy spectrum for the optimally doped composition consists of six CEF transitions out of the ground state $\Gamma_3^{(1)}$ [23]. These curves are denoted as A, B, C, D, E, and F. The Ca substitution results in the appearance of other spectral components denoted as A′, B′, C′, and

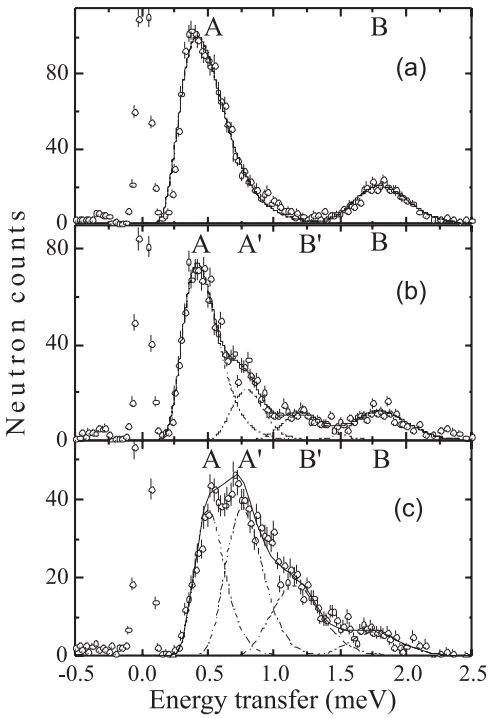

Figure 4. High-resolution scans of the lowest CEF transitions for the same $Ho_{1-y}Ca_yBa_2Cu_3O_{\approx 7}$ samples as in figure 3 ($T = 1.5$ K, $Q = 0.85$ Å^{-1}, $E_f = 3.5$ meV). The panels (*a*), (*b*), (*c*) correspond to $y = 0$, 0.1, 0.25, respectively. The curves are the result of a least-squares fitting procedure, using the log-normal function $f(x) = A\exp[-\ln^2(x/x_0)/2w^2]$ to approximate the lineshape of the CEF transitions. The CEF transitions are denoted as in figure 3.

D′, whose spectral weights distinctly increase with Ca content y. Since all the CEF levels of the Ho^{3+} ions in the orthorhombic symmetry are singlets, the decomposition of particular CEF transitions into two lines is direct experimental evidence for the existence of clusters, which make the system electronically inhomogeneous. This 'frustrated phase separation' was shown to be a characteristic feature of underdoped cuprates [17,22]. Our results demonstrate that the local electronic inhomogeneity in the CuO_2 planes still exists in the deeply overdoped regime.

From figures 3 and 4 we conclude that the energies and relative intensities of the curves A–F for the Ca-doped samples remain practically unchanged as compared to optimally doped Ho-123 (although the lines A, C, E, and F suffer some upward shift for the highest Ca content). Therefore, we identify these lines with the optimally doped clusters which persist in the samples under Ca doping, whereas the additional components A′, B′, C′, D′ are attributed to the overdoped clusters. The ratio $P_{undist} = [I_A + I_B]/[I_A + I_B + I_{A'} + I_{B'}]$ is a measure of the fractional proportion of the optimally doped, i.e. undisturbed, clusters, where I is the integral intensity of the corresponding line. Note, that the log-normal function was used to describe the highly asymmetric curve shape of the peaks in figure 4. The origin of this asymmetry was discussed in detail in [34]. From figure 4 we derive $P_{undist} = 0.74 \pm 0.03$ and 0.40 ± 0.03 for $y = 0.1$ and 0.25, respectively. Since the CEF is a local probe of the environment at the rare-earth sites [17, 26], one can assume that only the Ho^{3+} ions in the direct neighbourhood of an implanted Ca^{2+} ion are sensitive to the Ho^{3+} replacement by Ca^{2+}. Each Ho^{3+} ion has four nearest neighbours, which may be replaced by Ca^{2+}. Therefore, the statistical probability

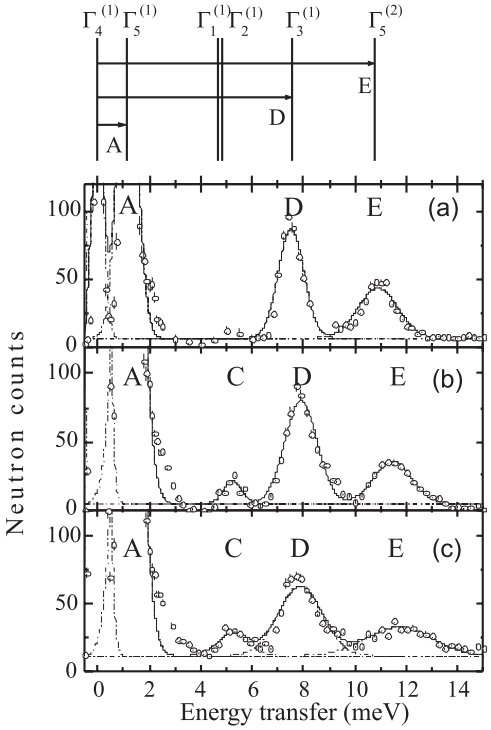

Figure 5. Energy spectra of neutrons scattered from $Ho_{1-y}Ca_yBa_2Cu_3O_{\approx 6.3}$ ($T = 1.5$ K, $Q = 1.8$ Å^{-1}, $E_f = 7$ meV) for $y = 0$, 0.1, 0.22 (in panels (*a*), (*b*), (*c*), respectively). The curves are the result of a least-squares fitting procedure (table 2) with use of Gaussian functions to describe the lineshape of the transitions. The top of the figure shows the CEF splitting of $HoBa_2Cu_3O_6$ [20], and the observed transitions are indicated by arrows.

of finding k of the four Ho sites ($0 \leqslant k \leqslant 4$) occupied by Ca is given by [22]

$$P_k^4(y) = \frac{4!}{(4-k)!k!} y^k (1-y)^{4-k}, \tag{1}$$

where y is the Ca concentration per formula unit. For the given Ca concentrations $y = 0.096 \pm 0.006$ and 0.246 ± 0.008 (table 1), equation (1) with $k = 0$ gives $P_{undist} = 0.67 \pm 0.03$ and 0.33 ± 0.03, respectively. These fractional proportions of undisturbed clusters are reasonably close to that derived above from our CEF data. This numerical analysis confirms the intrinsic origin of the superposition effect observed for the overdoped Ho-123 by the INS technique.

3.3. Underdoped regime

Energy spectra of neutrons scattered from $HoBa_2Cu_3O_{6.3}$, $Ho_{0.9}Ca_{0.1}Ba_2Cu_3O_{6.24}$, and $Ho_{0.78}Ca_{0.22}Ba_2Cu_3O_{6.32}$ at $T = 1.5$ K are shown in figure 5. Note that the transitions $\Gamma_4^{(1)} \rightarrow \Gamma_1^{(1)}$ and $\Gamma_4^{(1)} \rightarrow \Gamma_2^{(1)}$ are forbidden for the CEF of tetragonal symmetry. According to our findings discussed in section 3.2, we would expect the CEF transitions of the Ca-doped samples also to be composed of at least two spectral components associated with undoped and slightly doped clusters, respectively. Since Ca substitution produces a lowering of the local symmetry, we expect for the Ca-doped samples a splitting of the $\Gamma_5^{(1)}$ and $\Gamma_5^{(2)}$ doublets into

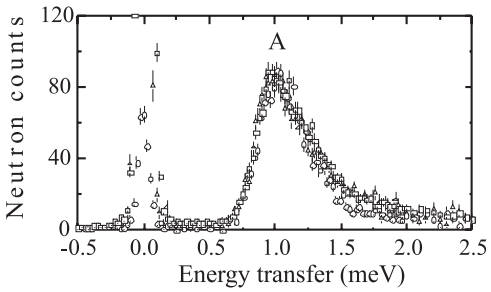

Figure 6. High-resolution scans of the lowest CEF transition A for the same $Ho_{1-y}Ca_yBa_2Cu_3O_{\approx 6.3}$ samples as in figure 5 ($T = 1.5$ K, $Q = 0.85$ Å^{-1}, $E_f = 3.5$ meV). Circles, squares, and triangles represent the data for $y = 0$, 0.1, and 0.22, respectively.

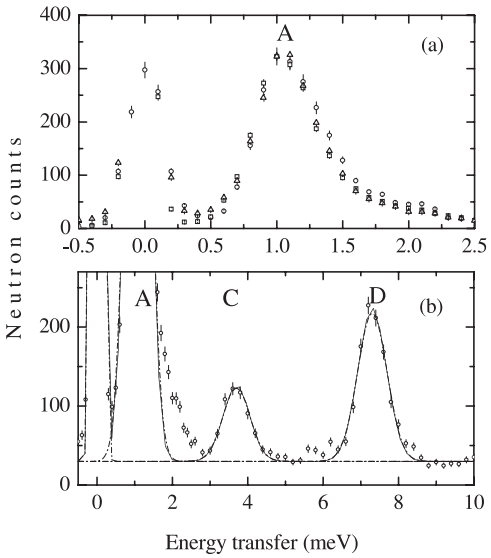

Figure 7. (*a*) The lowest CEF transition for $Ho_{1-y}Th_yBa_2Cu_3O_{6.3}$ samples measured at $T = 1.5$ K, $Q = 1.8$ Å^{-1}, $E_f = 5.6$ meV. Circles, squares, and triangles represent the data for $y = 0$, 0.07, and 0.13, respectively. (*b*) The energy spectrum of $Ho_{0.87}Th_{0.13}Ba_2Cu_3O_{6.3}$ measured at $T = 1.5$ K, $Q = 1.8$ Å^{-1}, $E_f = 5.6$ meV. The peak assignments refer to the CEF splitting scheme shown in figure 5. The curves represent a Gaussian fit to the observed CEF transitions.

two singlets as well as a finite intensity for the ground-state CEF transition $\Gamma_4^{(1)} \rightarrow \Gamma_1^{(1)}$ lying at ∼5 meV (the appearance of the curve C; see figure 3).

Figure 5 shows that the curve C is really observed for Ca-doped oxygen-deficient Ho-123, and its intensity is slightly raised with increasing Ca concentration. However, there is no evidence for superposition character of the spectra. Even the high-resolution low-energy scans displayed in figure 6 fail to reveal a splitting of the first excited doublet due to Ca substitution. Moreover, we failed to find any additional intensity in the high-resolution scans at the evaluation temperature $T = 10$ K indicative of a transition between the split levels of the $\Gamma_5^{(1)}$ doublet. We conclude therefore that curve C observed for the Ca-substituted samples with low oxygen concentration cannot be associated with doping by charge carriers. Due to the different ionic radii of Ho^{3+} and Ca^{2+}, one can assume line C to result from distortions of the copper–oxygen polyhedron around the Ho^{3+} ions in the immediate neighbourhood of the

implanted Ca^{2+} ions. However, due to the random orientation of the distorted copper–oxygen polyhedra, the average tetragonal symmetry of the sample is maintained, as concluded from the neutron powder diffraction experiments. On the other hand, such local distortions have an influence on the CEF interaction, since it is a local probe.

The INS measurements for the $Ho_{1-y}Th_yBa_2Cu_3O_x$ ($y = 0.07, 0.13$; $x \approx 6.3$) samples display the same features as were observed for the low-oxygen Ho-123 with Ca substitution (figure 7). Doping with Th does not produce a decomposition of the CEF transitions into different components, and the appearance of curve C is also observed with Th doping due to the lowering of the local symmetry around the Ho^{3+} ions.

4. Data analysis and discussion

4.1. Crystal-field calculations

Since the overall CEF splitting of the ground-state multiplet $^5I_8$ of the Ho^{3+} ions (∼74 meV) [23] is high enough as compared to the intermultiplet energy separation (∼620 meV for Ho^{3+}), the effect of both J-mixing and spin–orbit coupling (in the intermediate-coupling approximation) were shown to be important for correctly reproducing the observed energies and intensities of the CEF spectrum [21, 23]. Following [23], all the multiplets with $J = 8$, 7, and 6, lying at 0, 620, and 1067 meV, respectively, have been considered in our calculations. In order to find the CEF energy levels and wavefunctions of the Ho^{3+} ions, a simultaneous diagonalization of the electrostatic, spin–orbit, and CEF interactions has been performed. In this case the CEF Hamiltonian can be written in terms of tensor operators [35]:

$$H_{CEF} = \sum_{n=1}^{3}\sum_{m=0}^{n} B_{2m}^{2n}(C_{2m}^{2n} + C_{-2m}^{2n}), \tag{2}$$

where C_{2m}^{2n} are the spherical tensor operators and B_{2m}^{2n} are the CEF parameters to be determined from the experiment. For a crystal field of tetragonal symmetry, the CEF parameters with odd m vanish, while all nine CEF parameters are required for an orthorhombic symmetry.

To derive the CEF parameters B_{2m}^{2n} from the present INS experiments, least-squares fitting procedures, based on the differential neutron cross section, were applied to the observed energy spectra [36]:

$$\frac{\mathrm{d}^2\sigma}{\mathrm{d}\Omega\,\mathrm{d}\omega} \sim \frac{k_f}{k_i}F^2(Q)\sum_{i,j}\exp\left\{-\frac{E_i}{k_BT}\right\}|\langle\Gamma_j|J_p|\Gamma_i\rangle|^2\delta(E_j - E_i + \hbar\omega), \tag{3}$$

where $F(Q)$ is the magnetic form factor, E_i the energy of the ith CEF state with irreducible representation Γ_i, and J_p the component of the total angular momentum operator perpendicular to the scattering vector $\boldsymbol{Q}$. Using this procedure we calculated the CEF parameters

(i) for undoped $HoBa_2Cu_3O_{6.3}$ from the energy spectra shown in figures 5(*a*) and 6,
(ii) for optimally doped $HoBa_2Cu_3O_{6.95}$ from the energy spectra shown in figures 3(*a*) and 4(*a*), and
(iii) for the overdoped component of the Ca-substituted sample from the energy spectra displayed in figures 3(*c*) and 4(*c*) (lines A′, B′, C′, D′, E, and F).

The information on the high-energy part of the CEF spectrum ($55 < E < 75$ meV) was taken from [23], since the instrumental resolution is not sufficient to allow one to resolve additional spectral components. The results of the least-squares fitting procedure are listed in table 2 for the CEF energies and transition intensities. Rows 1–3 of table 3 demonstrate a general trend in the doping-induced variation of all the leading CEF parameters ($n = 1, 2, 3$; $m = 0, 2$) for

Table 3. CEF parameters B_{2m}^{2n} (meV) in Wybourne notation [31] of $Ho_{1-y}Ca_yBa_2Cu_3O_x$ derived in the present work.

$(2n, 2m)$	(2, 0)	(2, 2)	(4, 0)	(4, 2)	
1. $x = 6.3$, $y = 0$ (undoped)	30.6 ± 1.5	0	-272.1 ± 1.6	0	
2. $x = 6.95$, $y = 0$ (optimally doped component)	51.2 ± 2.6	11.6 ± 2.0	-271.8 ± 1.6	4.6 ± 1.0	
3. $x = 6.86$, $y = 0.25$ (overdoped component)	60.0 ± 3.0	2.0 ± 2.0	-256.8 ± 1.5	4.6 ± 1.0	
4. Derived from equation (6) $y = 0.25$,	—	—	-269.9 ± 1.6	—	
5. Derived from equation (7), $Z\|e\|\delta = 0.07$ hole/O	—	—	-260.5 ± 1.6	—	
	(4, 4)	(6, 0)	(6, 2)	(6, 4)	(6, 6)
1. $x = 6.3$, $y = 0$ (undoped)	151.3 ± 1.9	59.8 ± 1.2	0	173.4 ± 0.3	0
2. $x = 6.95$, $y = 0$ (optimally doped component)	153.2 ± 1.9	64.0 ± 1.2	-3.9 ± 2.0	176.1 ± 0.3	-0.4 ± 0.4
3. $x = 6.86$, $y = 0.25$ (overdoped component)	144.3 ± 1.7	49.6 ± 1.1	-3.9 ± 2.0	171.3 ± 0.3	-0.4 ± 0.4
4. Derived from equation (6), $y = 0.25$	149.4 ± 1.8	59.7 ± 1.3	—	173.4 ± 0.3	—
5. Derived from equation (7), $Z\|e\|\delta = 0.07$ hole/O	144.2 ± 1.8	57.1 ± 1.3	—	167.3 ± 0.3	—

$HoBa_2Cu_3O_x$, i.e., they increase when x goes from 6 to 7. A similar behaviour was also found for $ErBa_2Cu_3O_x$ [21]. For the Ca-free samples with low and high oxygen concentration, the CEF parameters are close to those published in [23].

4.2. Overdoped regime

In the point-charge approximation, the CEF parameters are explicitly given by

$$B_{2m}^{2n} = e|e|\langle r^{2n}\rangle \sum_i Z_i \gamma_{2m}^{2n}(i), \tag{4}$$

with

$$\gamma_{2m}^{2n}(i) = \frac{f_{2m}^{2n}(Q_i, \varphi_i)}{(r - R_i)^{2n+1}}. \tag{5}$$

The sum i runs over all neighbouring ions at positions R_i, $f_{2m}^{2n}(Q_i, \varphi_i)$ are tesseral harmonics, $\langle r^{2n}\rangle$ is the $2n$th moment of the radial distribution of the 4f electrons, Z_i is the charge of the ith ion in units of the electron charge $|e|$, and $\gamma_{2m}^{2n}(i)$ are geometrical coordination factors as defined by Hutchings [37]. In order to investigate whether the CEF parameters in the overdoped compounds $Ho_{1-y}Ca_yBa_2Cu_3O_7$ are controlled by structural modifications alone, we apply the following extrapolating procedure [21, 23]:

$$B_{2m}^{2n}(y) = \frac{\gamma_{2m}^{2n}(y)}{\gamma_{2m}^{2n}(0)} B_{2m}^{2n}(0), \tag{6}$$

where $\gamma_{2m}^{2n}(y)$ are geometrical coordination factors associated with the nearest-neighbour oxygen shell. We applied this procedure only to the leading fourth- and sixth-order parameters, since the second-order parameters are long-range parameters and the statistical uncertainty of the 'orthorhombic' parameters is rather large [23]. The set of CEF energies and transition intensities obtained (table 2, row 3) for $y = 0.25$ are clearly closer to the optimally doped set (table 2, row 2) than to the overdoped one (table 2, row 4). This means that structural

considerations alone can explain the Ca concentration behaviour of the optimally doped component (particularly the upward shift of curves A and C), but cannot reproduce the overdoped component of the spectra. We therefore conclude that the overdoped component is mainly due to hole doping of the CuO_2 planes. In order to quantify the associated charge transfer, we extend equation (6) by including the ligand charges $Z(y)$ of the nearest-neighbouring oxygen shell:

$$B_{2m}^{2n}(y) = \frac{Z(y)}{Z(0)} \frac{\gamma_{2m}^{2n}(y)}{\gamma_{2m}^{2n}(0)} B_{2m}^{2n}(0) \equiv (1-\delta) \frac{\gamma_{2m}^{2n}(y)}{\gamma_{2m}^{2n}(0)} B_{2m}^{2n}(0), \tag{7}$$

where $\delta(y) = 1 - Z(y)/Z(0)$ is the relative charge transfer. Taking the compound $HoBa_2Cu_3O_{6.95}$ as a reference (i.e., $Z(0) = -2$), we find that an additional charge of $Z|e|\delta \sim 0.07$ hole/O, i.e. $\sim$0.14 hole/plane, has to be transferred into the CuO_2 planes upon $y = 0.25$ Ca doping in order to reproduce the CEF splitting observed for the overdoped clusters (table 3, row 5).

It is worth mentioning that when the charges are segregated into microscopic domains, any increase of the doping level does not affect the local charge density in the domains, but increases the volume fraction of the domains with the higher hole concentration, i.e., the spectral weight of the overdoped component of the CEF spectrum is enhanced (see figures 3 and 4). According to the present results, this 'two-phase' picture, established earlier for the underdoped region [17,22], is also applicable to the overdoped regime. In particular, there is a smooth crossover between the underdoped and overdoped regions of the phase diagram. This conclusion is in qualitative agreement with recent results of an inelastic neutron scattering study of high-energy longitudinal optical phonons for $YBa_2Cu_3O_x$ [38], indicative of strong charge inhomogeneity even for the optimally doped compound with $x = 6.93$. Note that the CEF interaction probes a time-averaged (static) component of the charge distribution. Therefore, in $HoBa_2Cu_3O_{6.95}$ near optimal doping, the superposition character of the CEF vanishes due to a negligible difference between the averaged and local charge-carrier concentration.

Since substitution of Ca^{2+} ions for Ho^{3+} ions increases the volume fraction of the overdoped domains, the hole concentration averaged over the sample volume increases with Ca content. The averaged hole concentration $\langle n \rangle$ for each Ca-doped sample can be estimated by the value of V_- [39] calculated from the structural data via the bond valence sums [40] for Cu(2), O(2), and O(3) ions (table 1). We obtain the values $n_{opt} = 0.19 \pm 0.01$ (hole/plane) and $\langle n \rangle = 0.23 \pm 0.01$ (hole/plane) for optimally doped $HoBa_2Cu_3O_{6.95}$ and overdoped $Ho_{0.9}Ca_{0.1}Ba_2Cu_3O_{6.99}$, respectively. Note that these results agree well with the in-plane hole concentration derived from site-specific x-ray absorption spectroscopy, $n_{opt} = 0.20$ and $\langle n \rangle = 0.245$, for $YBa_2Cu_3O_{6.91}$ and $Y_{0.9}Ca_{0.1}Ba_2Cu_3O_{6.91}$, respectively [41]. To estimate the hole concentration of the overdoped clusters n_{over} in $Ho_{1-y}Ca_yBa_2Cu_3O_7$, a simple two-phase relation can be used:

$$n_{over} = \frac{\langle n \rangle - P_{undist} n_{opt}}{1 - P_{undist}}. \tag{8}$$

From table 1 and equation (8) we obtain $n_{over} = 0.34 \pm 0.06$ hole/plane and $n_{over} = 0.30 \pm 0.03$ hole/plane for $Ho_{0.9}Ca_{0.1}Ba_2Cu_3O_{6.99}$ ($P_{undist} = 0.74$) and $Ho_{0.75}Ca_{0.25}Ba_2Cu_3O_{6.86}$ ($P_{undist} = 0.4$), respectively. The difference $\Delta n_{Ca-induced} = n_{over} - \langle n_{opt} \rangle \approx 0.13$ hole/plane is another quantitative estimate of the Ca-induced overdoping in the CuO_2 planes, which agrees perfectly with our CEF considerations based on equation (7).

4.3. Underdoped regime

Our experiments do not provide evidence for doping with charge carriers for Ca- and Th-substituted Ho-123 with low oxygen concentration. We note first that these samples have no

superconductivity, like the Ca-doped low-oxygen Y-123 samples studied by Merz *et al* [41]. However, for the latter compounds, Ca-induced doping of the planes was observed, while we did not observe this. Perhaps this discrepancy results from different technologies used to produce oxygen-deficient samples. Our oxygen-deficient samples were prepared by a quenching technology. Quenching may cause rather strong local disorder, which prevents the CuO_2 plane from be properly doped with charge carriers. The undoped character of our low-oxygen samples with Ca substitutions is confirmed by the calculated effective hole concentration V_- [39] (table 1). In fact, the values of V_- remain unchanged for all the low-oxygen samples within the experimental accuracy. Therefore, our results are consistent in the sense that the absence of superconductivity corresponds to undoped character of the CEF spectra in the low-oxygen Ho-123 samples with Ca substitution.

5. Conclusions

Charge distribution resulting from the in-plane doping with charge carriers was probed by means of neutron spectroscopy of the CEF interaction in the high-T_c superconductor $HoBa_2Cu_3O_x$ at low and high oxygen concentrations. The in-plane doping was induced either by substitution of Ca^{2+} ions or Th^{4+} ions for Ho^{3+} ions. For the oxygen-rich $Ho_{1-y}Ca_yBa_2Cu_3O_x$ samples ($x = 6.99$, $y = 0.1$; $x = 6.86$, $y = 0.25$) the CEF spectra were found to be decomposed into two spectral components. Since all the CEF levels of the Ho^{3+} ions in the orthorhombic symmetry are singlets, such a decomposition is direct experimental evidence for the existence of clusters which make the system electronically inhomogeneous. Therefore, the 'two-phase' picture established earlier for the underdoped regime is conserved in the overdoped regime of the Ho-123 high-T_c superconductor, with a smooth crossover between the underdoped and overdoped parts of the phase diagram.

For the oxygen-deficient samples with both Ca^{2+} (positive-doping) and Th^{4+} (negative-doping) substitutions for Ho sites, we found only specific deformations of the CEF spectra resulting from distortions of the copper–oxygen polyhedra around the Ho^{3+} ions, rather than from the doping-induced variation of the carrier concentration in the CuO_2 planes.

Acknowledgments

We thank A Karkin for resistivity measurements, V Kozhevnikov and B Goshchitskii for helpful discussions. Financial support by the Russian Foundation for Basic Research (project No 00-02-17370), Commission of Russian Academy of Sciences for Young Scientists Support (6th competition, grant No 67), Russian State Programmes 'Neutron Investigation of Condensed Matter' (State contract No 107-19(00)—P-D01) and 'Superconductivity' (State contract No 107-1(00)—P-D01, agreement No 7/01) is gratefully acknowledged.

References

[1] Emery V J and Kivelson S A 1995 *Nature* **374** 434
[2] Salkola M I, Emery V J and Kivelson S A 1996 *J. Supercond.* **9** 401
[3] Zaanen J and van Saarloos W 1997 *Physica* C **282–7** 178
[4] Castro-Neto A H and Hone D 1996 *Phys. Rev. Lett.* **76** 2165
[5] Castellani C, di Castro C and Grilli M 1996 *J. Supercond.* **9** 413
[6] Hammel P S and Scalapino D J 1996 *Phil. Mag.* B **74** 523
[7] Tranquada J M, Sternlieb B J, Axe J D, Nakamura Y and Uchida S 1995 *Nature* **375** 561
[8] Tranquada J 1998 *Physica* B **241–3** 745
[9] Aeppli G, Mason T E, Hayden S M, Mook H A and Kulda J 1997 *Science* **278** 1432

[10] Cheong S-W, Hwang H Y, Chen C H, Batlogg B, Rupp L W and Carter S A 1994 *Phys. Rev.* B **49** 7088
[11] Hammel P C, Reyes A P, Cheong S-W, Fisk Z and Schriber J E 1993 *Phys. Rev. Lett.* **71** 440
[12] Yamada K, Lee C H, Endoh Y, Shirane G, Birgeneau R J and Kastner M A 1997 *Physica* C **282–7** 85
[13] Kataev V, Rameer B, Vavilov A, Büchner B, Hücker M and Borowski R 1998 *Phys. Rev.* B **58** R11 876
[14] Bianconi A, Valetta A, Perali A and Saini N L 1997 *Solid State Commun.* **102** 369
[15] Bianconi A, Lusignoli M, Saini N L, Bordet P, Kvik Å and Radaelli P G 1996 *Phys. Rev.* B **54** 4310
[16] Saini N L, Lanzara A, Bianconi A and Oyanagi H 1998 *Phys. Rev.* B **58** 11 768
[17] Mesot J and Furrer A 1997 *J. Supercond.* **10** 623
[18] Goodman G L, Loong C K and Soderholm L 1991 *J. Phys.: Condens. Matter* **3** 49
[19] Soderholm L, Loong C K and Kern S 1992 *Phys. Rev.* B **45** 10 062
[20] Boothroyd A T, Doyle S M and Osborn R 1993 *Physica* C **217** 425
[21] Mesot J, Allenspach P, Staub U, Furrer A, Mutka H, Osborn R and Taylor A 1993 *Phys. Rev.* B **47** 6027
[22] Mesot J, Allenspach P, Staub U, Furrer A and Mutka H 1993 *Phys. Rev. Lett.* **70** 865
[23] Staub U, Mesot J, Guillaume M, Allenspach P, Furrer A, Mutka H, Bowden Z and Taylor A 1994 *Phys. Rev.* B **50** 4068
[24] Boothroyd A T, Mukherjee A and Murani A P 1996 *Phys. Rev. Lett.* **77** 1600
[25] Rubio Temprano D, Mesot J, Janssen S, Conder K, Furrer A, Mutka H and Müller K A 2000 *Phys. Rev. Lett.* **84** 1990
[26] Böttger G 1996 Investigation of high-temperature superconductors of the R–Ba–Cu–O family: substitution effects and magnetic properties *PhD Thesis* ETH Zurich
[27] Böttger G, Mesot J, Fischer P and Furrer A 1997 *Physica* B **234–6** 843
[28] Tokura Y, Torrance J B, Huang T C and Nazzal A I 1988 *Phys. Rev.* B **38** 7156
[29] Lundqvist P, Grahn P, Rapp O and Bryntse I 1997 *Physica* C **289** 137
[30] Tallon J L, Bernhard C, Shaked H, Hitterman R L and Jorgensen J D 1995 *Phys. Rev.* B **51** 12 911
[31] Fisher B, Genossar J, Kuper C G, Patlagan L, Reisner G M and Knizhnik A 1993 *Phys. Rev.* B **47** 6054
[32] Rodriguez-Carvajal J 1993 *Physica* B **192** 55
[33] Podlesnyak A, Mirmelstein A, Golosova N, Bobrovskii V, Mitberg E, Conder K and Furrer A 2002 at press
[34] Henggeler W, Guillaume M, Allenspach P, Mesot J, Furrer A and Adams M 1999 *J. Phys.: Condens. Matter* **11** 2921
[35] Wybourne B G 1965 *Spectroscopic Properties of Rare Earths* (New York: Interscience)
[36] Trammell G T 1953 *Phys. Rev.* **92** 1387
[37] Hutchings M T 1964 *Solid State Physics: Advanced Research and Applications* ed F Seitz and D Turnbull (New York: Academic) **16** 227
[38] Petrov Y, Egami T, McQueeney R J, Yethiraj M, Mook H A and Dogan F 2000 *Preprint* cond-mat/0003414
[39] Tallon J 1990 *Physica* C **168** 85
[40] Altermatt D and Brown I D 1985 *Acta Crystallogr.* B **41** 240
[41] Merz M *et al* 1998 *Phys. Rev. Lett.* **80** 5192